International Journal of Applied Power Engineering (IJAPE)
Vol. 15, No. 3, September 2026, pp. 1132~1146
ISSN: 2252-8792, DOI: 10.11591/ijape.v15.i3.pp1132-1146

Fuzzy logic based intelligent control of active front end converter for five phase voltage source inverter fed induction motor drive

C. Kalaivani[1], D. Raja[2], S. Sivasakthi[3], R. Gnanaselvam[4]
[1]Department of Electrical and Electronics Engineering, AMET University, Chennai, India
[2]Department of Electrical and Electronics Engineering, Sri Manakula Vinayagar Engineering College, Puducherry, India
[3]Department of Electrical and Electronics Engineering, Krishnasamy College of Engineering and Technology, Cuddalore, India
[4]Department of Electronics and Communication Engineering, Karpaga Vinayaga College of Engineering and Technology, Karpaga Vinayaga Educational Lore for Learning (Deemed to be University), Chengalpattu, India

Article Info

Article history:

Received Aug 24, 2025
Revised Apr 3, 2026
Accepted Jun 9, 2026

Keywords:

5-ϕ induction motor
Active front end converter
Fuzzy logic control
Space vector PWM
Unity power factor

ABSTRACT

This paper deals with an active front-end converter (AFEC) for a 5-ϕ inverter-fed induction motor (IM) drive. Multi-phase IM drive stands as an evolving domain of electrical drive usages. Supply from the grid is prone to be unbalanced and affects the input power quality of adjustable multi-phase IM drives. This work proposes a fuzzy logic control strategy with the space vector pulse width modulation (SVPWM) switching scheme for the AFEC outer voltage control along with inner current control loops for attenuating the disturbances due to voltage unbalance conditions. This method of control can keep the power factor nearby unity on the AC side with sinusoidal AC current and constant DC voltage at the DC link capacitor. A 5-ϕ inverter designed with SVPWM for IM drive enables operation of the drive with reduced percentage total harmonic distortion (THD) in the voltage of output side. This SVPWM control for a 5-ϕ voltage source inverter (VSI) uses entire voltage of the DC bus and the output responses are more efficient having a minimal lower order THD. The dynamic performances of a 5-ϕ VSI fed IM drive are investigated. The simulation results show the system has an improved power factor at the front-end, constant DC voltage across the capacitor, low THD at the input current, and a superior output performance for the 5 phase IM based drive.

Corresponding Author:

C. Kalaivani
Department of Electrical and Electronics Engineering, AMET University
Chennai, India
Email: dr.kalaivani@amet-ist.in

1. INTRODUCTION

Multi-phase drives hold numerous advantages over 3-ϕ drives and are utilized in applications due to several benefits in the automotive, aviation, and electric power generation sectors. When there are even numbers of phases, the poles coincide alongside each other, reducing motor functioning. Hence, odd numbers of phases are chosen instead of even amount of phases [1], [2]. Also, the 5-ϕ induction motor (IM) has superior fault tolerance ability as compared with the 3-ϕ system, diverting attention to the development of multiphase machine control for industry applications [3]-[5].

Nonlinear loads such as variable speed IM drives are the source of harmonics in current, which produce reactive power and losses in the transmission line. It requires power factor correction (PFC) converters to limit the input current harmonics of modern variable speed drives (VSDs) as per IEEE519, IEC1000-3-2, and EN61000-3-2. Research interest in this form of pulse width modulation (PWM) converter has developed rapidly over the past few years and various techniques have been proposed in the literature [6]-[8]. Design of direct power control (DPC) and DPC-space vector modulation (SVM) techniques for 3-ϕ PWM converters led to input side power quality improvement [9]-[15].

The fuzzy controller is an alternative solution to the PI controller and it is proposed for switched reluctance motor speed regulation. Its performance is found to be satisfactory compared to the conventional PI controller [16]. The selective harmonic elimination methods are proposed for high power electric drive with the goal to improve the system's power quality [17]-[20]. However, problems with input side power quality, including flicker, swell, and sag in the voltage, should be considered while designing the control algorithm for AFEC.

In this paper, dual control strategies with (space vector PWM) SVPWM are used to improve the line current quality at the AC input supply with unity PF and constant DC link voltage for IM drives. In the front-end decoupled control, fuzzy controller works better than PI controllers to achieve better dynamic performance. The SVPWM scheme generates the trigger pulses for IGBT switches in the AC-DC converter to have total control of input current total harmonic distortion (THD), reactive power, and DC bus potential. The SVPWM switching scheme is presented with regard to the 5-ϕ VSI-fed drive. This control uses the entire voltage of the DC bus and the output responses are more efficient having a marginally lower order THD.

2. VOLTAGE SAGS ON VSDS

Unwanted tripping of the equipment depends on both unbalanced voltage and phase angle shift. The voltage sags in the AC input supply point is due to various faults in the power system. Voltage sag classification according to IEEE 1159 standards is given in Table 1.

The VSD comprises a front end converter, a DC bus and an inverter. Different types of sags may appear in the power system and it will disturb the performance of VSDs [21]. VSD performance depends on the hardware, software for the controller, and response time of a control system. The DC link may supply the energy during short sags, but for the longer sags the capacitor voltage reduces to a lower level and it cannot supply the energy. So, the inverter will trip during this condition. Analysis of instantaneous voltage sag and its mitigation are considered for the 5-ϕ IM drive.

Table 1. Voltage sag categorization

Type of sag	Duration	Magnitude (pu)
Instantaneous	0.01-0.4 sec	0.1 - 0.9
Momentary	0.4-3 sec	0.1 - 0.9
Temporary	3-1 min	0.1 - 0.9

3. ACTIVE FRONT-END CONVERTER FOR FIVE-PHASE IM DRIVE

Decoupled control is necessary, similar to DC motor control, to achieve good dynamic performance in the line side of an AC to DC converter. This decoupled control is possible only by the vector control method. The primary objective of vector control remains to transform the 3-ϕ quantities into 2-ϕ quantities. Here, input currents i_a, i_b and i_c are converted into i_q and i_d parameters. Reactive power is regulated through the i_q parameter, and DC capacitor voltage in the DC link by the i_d parameters. The feedback and forward control help to obtain a faster dynamic response.

There are certain power quality issues related to adjustable speed drives which need to be controlled at the front end of the IM drive system. The circuit in Figure 1 shows that the basic structure of a 3-ϕ PFC converter for a 5-ϕ IM drive consists of a dual closed loop including forward path, feed-forward control, and feedback control. The 3-ϕ quantities are transformed to 2-ϕ quantities for the purpose of decoupled control by sensing the 3-ϕ currents and voltages from the supply. SVPWM receives the αβ components to produce gate signals that are fed to the converter.

3.1. Mathematical representation of front-end converter

The basic current relationship is given by (1). PWM converter input voltages can be described as (2)-(4).

$$i_a + i_b + i_c = 0 \tag{1}$$

$$V_a = L\frac{di_a}{dt} + R\, i_a + V_{ra} \tag{2}$$

$$V_b = \mathrm{L}\frac{di_b}{dt} + Ri_b + Vr_b \tag{3}$$

$$V_c = L\frac{di_c}{dt} + Ri_c + Vr_c \tag{4}$$

Input line voltages of a PWM converter is given as (5)-(7).

$$V_{ra} = [S_a - \frac{1}{3}(S_a + S_b + S_c)]\, V_{dc} \tag{5}$$

$$V_{rb} = [S_b - \frac{1}{3}(S_a + S_b + S_c)]\, V_{dc} \tag{6}$$

$$V_{rc} = [S_c - \frac{1}{3}(S_a + S_b + S_c)]\, V_{dc} \tag{7}$$

The 3-ϕ system voltage equation under balanced condition is as (8)-(10).

$$v_L = v_I + v_S \tag{8}$$

$$V_L = Ri_L + L\frac{di}{dt} + V_S \tag{9}$$

$$\begin{bmatrix} V_a \\ V_b \\ V_c \end{bmatrix} = R \begin{bmatrix} i_a \\ i_b \\ i_c \end{bmatrix} + L\frac{d}{dt}\begin{bmatrix} i_a \\ i_b \\ i_c \end{bmatrix} + \begin{bmatrix} V_{sa} \\ V_{sb} \\ V_{sc} \end{bmatrix} \tag{10}$$

In addition, for currents (11).

$$C\frac{dV_{dc}}{dt} = S_a i_a + S_b i_b + S_c i_c - i_L \tag{11}$$

The park coordinate transformation is used to obtain synchronous d-q coordinate equation [9].

$$P = \frac{2}{3}\begin{bmatrix} \cos\theta & \cos\left(\theta - \frac{2\pi}{3}\right) & cos\left(\theta + \frac{2\pi}{3}\right) \\ \sin\theta & \sin\left(\theta - \frac{2\pi}{3}\right) & sin\left(\theta + \frac{2\pi}{3}\right) \\ 0.5 & 0.5 & 0.5 \end{bmatrix} \tag{12}$$

$$L\frac{di_d}{dt} = v_d - Ri_d + \omega L i_q - v_{rd} \tag{13}$$

$$L\frac{di_q}{dt} = v_q - Ri_q + \omega L i_d - v_{rq} \tag{14}$$

$$C\frac{dV_{dc}}{dt} = \frac{3}{2}(S_d i_d + S_q i_q) - \frac{V_{dc}}{R_L} \tag{15}$$

Where:

$$S_d = S_\alpha \cos \omega t + S_\beta \sin \omega t \tag{16}$$

$$S_q = S_\beta \cos \omega t + S_\alpha \sin \omega t \tag{17}$$

$$v_{rd} = S_d V_{dc} \tag{18}$$

$$v_{rq} = S_q V_{dc} \tag{19}$$

v_{rd}, v_{rq} and S_d, S_q are input voltages of rectifier, switching function in synchronous rotating d-q coordinate, respectively. v_d, v_q *and* i_d, i_q are voltages and currents in synchronous rotating d-q coordinate, respectively, and ω is the angular frequency.

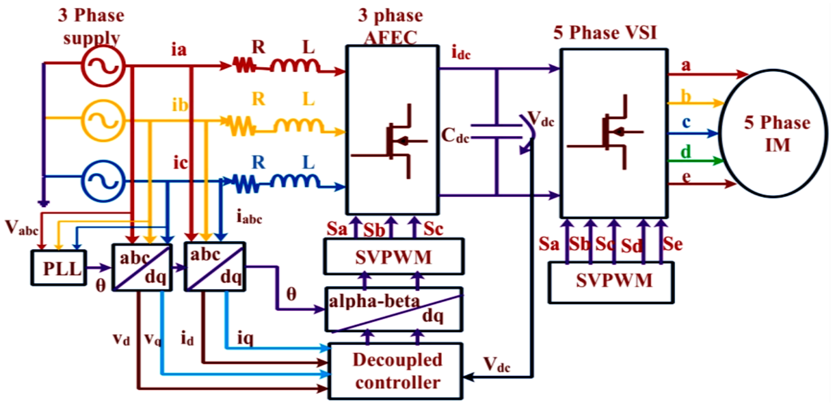

Figure 1. Active front-end converter for 5-ϕ IM drive

4. CONTROL STRATEGIES FOR AFEC

Voltage and virtual-based control are the 2 control strategies used for AFEC. In this paper, voltage based control is used for the PWM generation. The inner current loop of the VOC scheme is designed in such a way that it should give the best static and dynamic performance of internal control loops.

Figure 2 shows the voltage oriented d-q coordinate transformation, in that the AC input current i_L is divided into $i_L = [i_{Ld}, i_{Lq}]$, two rectangular components. The i_{Lq} part decides the reactive power, whereas the i_{Ld} part determines an active power flow. Hence, the two powers (real and reactive) are regulated independently.

The circuit achieves the unity power factor condition during the alignment of i_L and v_L. An (20) and (21) gives the simplified dynamic model of d-q synchronous frame voltage equations.

$$V_{Ld} = Ri_{Ld} + L\frac{di_{Ld}}{dt} + V_{sd} - \omega L i_{Lq} \quad (20)$$

$$V_{Lq} = Ri_{Lq} + L\frac{di_{Lq}}{dt} + V_{sq} - \omega L i_{Ld} \quad (21)$$

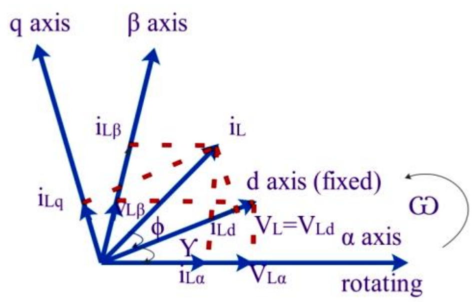

Figure 2. Phasor diagram of d-q to α-β co-ordinates transformation in VOC

Decoupled current control is essential for the AFEC to achieve high performance with accurate current tracking [9]. Figure 3 shows the flow diagram of such a decoupled current control for the AFEC. Real power and reactive power reference frame controls are referred to as i_d and i_q controls, respectively. DC link voltage steadiness shall be achieved by active power V_{dc} control loop as well as the power factor by the reactive power inner current control loop.

$$V_{sd} = \omega L i_{Lq} + V + \Delta v_d \quad (22)$$

$$V_{sq} = \omega L i_{Lq} + \Delta v_q \quad (23)$$

Here, the output of current controllers is as (24) and (25).

$$\Delta V_d = k_p(i_d^* - i_{d)+} k_i \int (i_d^* - i_d)\, dt \quad (24)$$

$$\Delta V_q = k_p(i_q^* - i_{q)+} k_i \int (i_q^* - i_q)\, dt \quad (25)$$

From (24) and (25), k_p and k_i represent the proportional and integral controller gains, respectively. The outputs of the PI controller are then transformed into the dq reference frame. These transformed outputs are subsequently used to generate the converter firing pulses through space vector modulation.

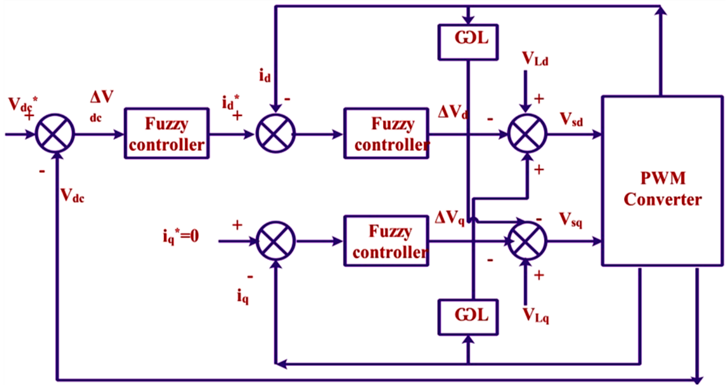

Figure 3. Decoupled current control for front-end PWM converter

4.1. Fuzzy logic controllers

The fuzzy logic controller (FLC) is non-linear and adjusts its control signal according to the changes in the input and output disturbances. Here, a Mamdani type fuzzy based control is used in the outer control loop of voltage to improve the DC link voltage steadiness, and an inner control of current for power factor improvement through the reactive power control. Input and output variables of fuzzy controllers use a 5×5 triangular membership function [16]. The well-defined rule base is presented in Table 2. The membership values are tuned to give the best control performance.

Table 2. Fuzzy rule base

Input variables		Error (e)				
Change in error (de)		NL	NS	Z	PS	PL
	NL	NL	NL	NS	NS	Z
	NS	NL	NS	NS	Z	PS
	Z	NS	NS	Z	PS	PS
	PS	NS	Z	PS	PS	PL
	PL	Z	PS	PS	PL	PL

‘e’ and ‘de’ are the two inputs to the controllers. Three FLC are used for the decoupled control, one aimed at the voltage control of outer DC link and the other two in the inner loop for reactive power control through which the UPF and pure sinusoidal current in input can be achieved. The controllers are designed with the triangular membership function and used for outer voltage control loop and inner current control loop, shown in Figures 4 and 5, respectively. The range for ‘e’ is -3 to 1 and for 'de' is -0.3 to 0.15, whereas for the controller output, it is -30 to 30 for the outer voltage control loop. The range for 'e' is -0.6 to 3.5 and for 'de' is -0.2 to 0.2, whereas for the output, it is 195 to 200 for the inner current controllers.

The rules are designed, resulting in a symmetrical matrix. The rule base of FLC system is represented by: If ‘e(t)’ is ‘PL’ and ‘de(t)’ is ‘Z’ then ‘c’ is ‘PS’.

$$\mathrm{e} = \mathrm{V_{dc}} - \mathrm{V_{dcref}} \tag{26}$$

$$\mathrm{de} = \mathrm{e_k} - \mathrm{e_{k-1}} \tag{27}$$

$$U(t) = f(e(t), de(t)) \tag{28}$$

Where f is the fuzzy logic control function that relates the error and change in error to the control output. The max-min inference method is utilized (29) to map the fuzzified values to the output fuzzy variables c(t) out of different inference algorithms.

$$\mu_c(z) = \max_{i=1..n}\left[\min(\alpha_i, \mu_c(z))\right] \tag{29}$$

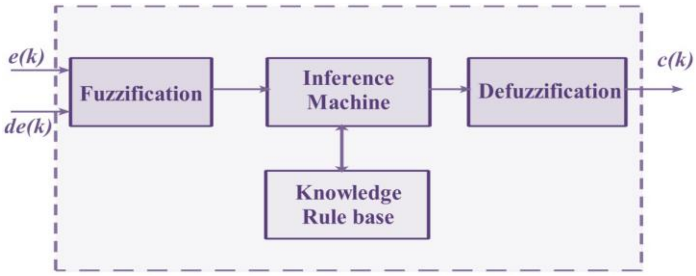

Figure 4. General FLC rule base system

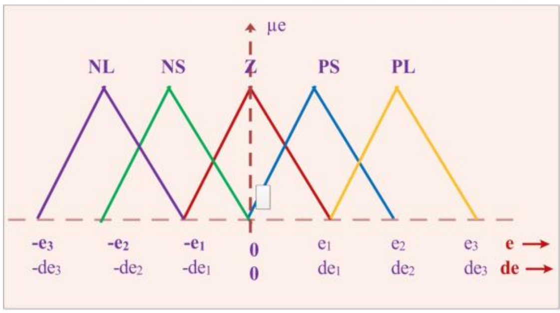

Figure 5. FLC membership functions for both speed error (e) and previous state speed error (de)

5. PWM TECHNIQUES

The SVPWM control structure is presented in Figure 6. One switching cycle is divided into 8 states (V_0 to V_7) out of which 6 are active (V_1 upto V_6) and 2 are zero conditions (V_0 and V_7). The reference vector V_r is calculated, and it rotates over 360 degrees in all sectors. V_r travel in angle Θ depends on switching frequency. Here, the SVPWM is used and the responsibilities are as follows:

- To sustain a constant and regulate the voltage in DC link with regard to changes in load and unbalance in the supply network.
- To minimize harmonics injected by the rectifier switching in the line side, and to provide UPF at the supply point.

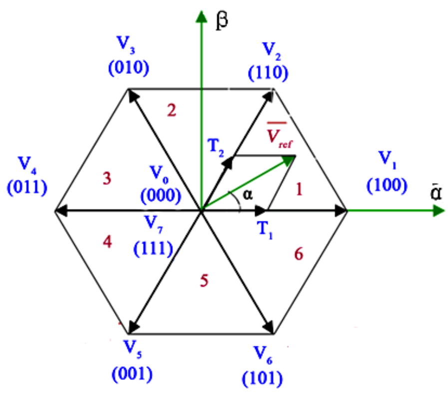

Figure 6. Space vector representation for the SVPWM technique

6. FIVE PHASE VSI WITH SVPWM CONTROL

The 5-ϕ 2-level VSI and its SVPWM control are shown in Figures 7 and 8. It can be represented in the (d_1-q_1) space vector plane, which contains two zero vectors and thirty active vectors. The inverter has 32 switching state combinations (i.e., 2^n, where $n$is the number of phases) [22]–[25].

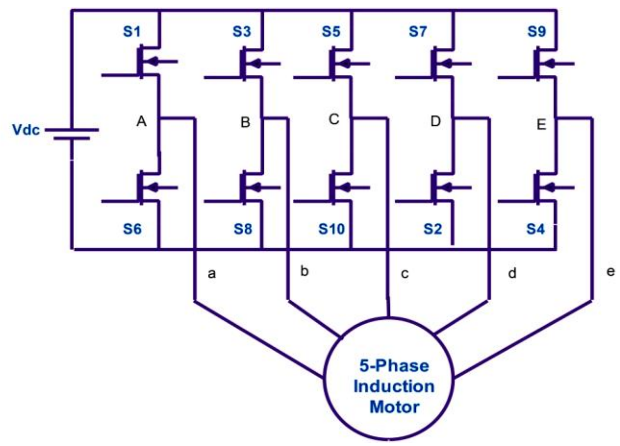

Figure 7. 5-ϕ VSI fed IM drive

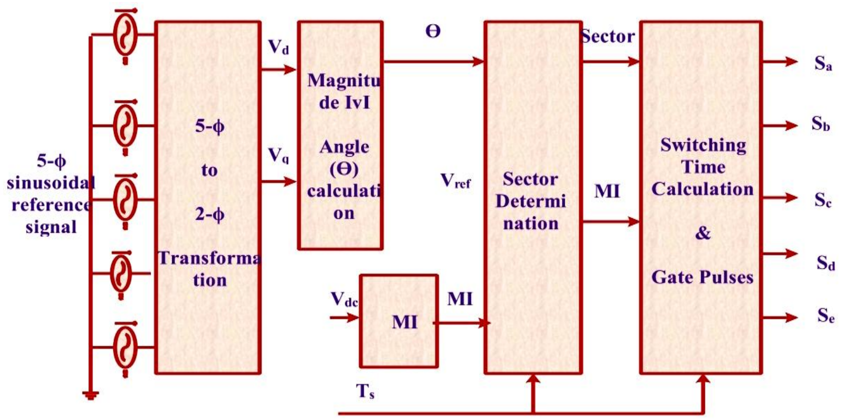

Figure 8. SVPWM control for 5-ϕ 2-level VSI

Inverter pole voltages could be used to express the 5-ϕ VSI's phase to neutral voltages ($V_a \sim V_e$) as shown in (30) and (31) [12].

$$V_j = \frac{4}{5}\mathrm{V_j} - \frac{1}{5}\sum_{\mathrm{i,i\neq j}}^{5}\mathrm{V_j},\ \text{ if j} < 5 \tag{30}$$

$$V_j = \frac{4}{5}\mathrm{V_j} - \frac{1}{5}\sum_{\mathrm{i,i\neq j}}^{4}\mathrm{V_j},\ \text{ if j} = 5 \tag{31}$$

In (28) indicates the 5-ϕ inverter voltages in 2-ϕ d-q plane. The value of $\mathrm{a}, \mathrm{a}^2, \mathrm{a}^3$ and a^4 are donated by (32) to (36).

$$V_{d1q1} = \frac{2}{5}\mathrm{V_{dc}}[\mathrm{V_a} + \mathrm{aV_b} + \mathrm{a^2V_c} + \mathrm{a^3V_d} + \mathrm{a^4V_e}] \tag{32}$$

$$\mathrm{a} = \cos\frac{2\pi}{5} + \sin\frac{2\pi}{5} \tag{33}$$

$$\mathrm{a}^2 = \cos\frac{4\pi}{5} + \sin\frac{4\pi}{5} \tag{34}$$

$$\mathrm{a}^3 = \cos\frac{4\pi}{5} - \sin\frac{4\pi}{5} \tag{35}$$

$$\mathrm{a}^4 = \cos\frac{2\pi}{5} - \sin\frac{2\pi}{5} \tag{36}$$

The two zero vectors are the starting point for the 3 coordinated decagons made up of the thirty active vectors, and are shown in Figure 7. Inner, center, and outer decagon values are 0.2472, 0.4, and 0.6472, respectively. Tables 3 and 4 present magnitudes and phase angles of the vectors in d-q plane, which are calculated using (37).

$$V_{d1q1} = \frac{2}{5} V_{dc}[V_a + aV_b + a^2V_c + a^3V_d + a^4V_e] \quad (37)$$

The d_1q_1 plane's large decagon's space vectors are taken into account. As illustrated in Figure 9, the switching vector travels counter-clockwise from V25 to V17 to the neighboring space vector. The operation time for every switching state is determined using (38) to (40) and is displayed in Figure 10. The following formulas are used to determine every switching state's conduction period.

$$t_{al} = \frac{|V_{ref}|\sin\left(\left(K\frac{\pi}{5}\right)-\theta\right)}{V_l \sin\left(\frac{\pi}{5}\right)} t_s \quad (38)$$

$$t_{bl} = \frac{|V_{ref}|\sin\left(\theta-\left((K-1)\frac{\pi}{5}\right)\right)}{V_l \sin\left(\frac{\pi}{5}\right)} t_s \quad (39)$$

$$t_0 = \frac{t_s - t_{al} - t_{bl}}{2} \quad (40)$$

Large space vector's highest feasible fundamental voltage peak is as (41).

$$V_{max} = |V_l|\cos\frac{\pi}{10} V_{dc} = 0.6155V_{dc} \quad (41)$$

Table 3. Magnitude and phase angle of vectors in d-q plane for decimal value 1-15

Decimal value	Equivalent binary number	d-q plane	
		Magnitude (pu)	Angle (degree)
0	00000	0	0
1	00001	0.4	-72
2	00010	0.4	-144
3	00011	0.6472	-108
4	00100	0.4	144
5	00101	0.2472	-144
6	00110	0.6472	180
7	00111	0.6472	-144
8	01000	0.4	72
9	01001	0.2472	0
10	01010	0.2472	144
11	01011	0.2472	-108
12	01100	0.6472	108
13	01101	0.2472	108
14	01110	0.6472	144
15	01111	0.4	180

Table 4. Magnitude and phase angle of vectors in d-q plane for decimal value 16-31

Decimal value	Equivalent binary number magnitude (pu)	d-q plane	
16	10000	0.4	0
17	10001	0.6472	-36
18	10010	0.2472	-72
19	10011	0.6472	-72
20	10100	0.2472	72
21	10101	0.2472	-36
22	10110	0.2472	180
23	10111	0.4	-108
24	11000	0.6472	36
25	11001	0.6472	0
26	11010	0.2472	36
27	11011	0.4	-36
28	11100	0.6472	72
29	11101	0.4	36
30	11110	0.4	108
31	11111	0	135

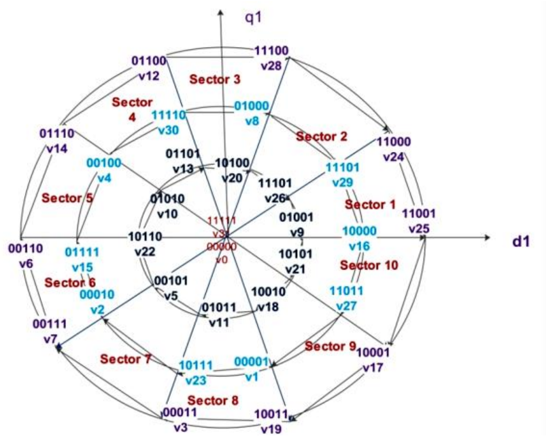

Figure 9. Switching states of d_1-q_1 subspace

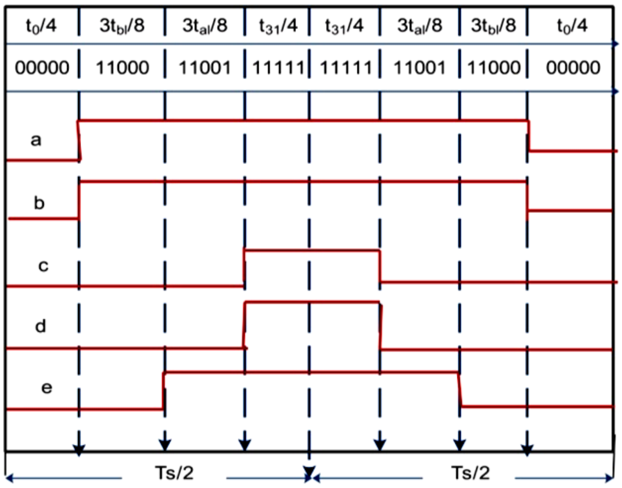

Figure 10. Switching sequences for large vectors of d_1-q_1 sub-space

7. SIMULATION RESULTS

MATLAB/Simulink has been employed to develop the AFEC for the five phase VSI controlled IM drive and the specifications are given in Table 5. The 3-ϕ RMS input line voltage is 415 V, 50 Hz. The DC link capacitor is 560 µF and the line value of inductance is 7 mH. In the steady state, the DC output potential is 400 V and 3 kHz is taken as the switching frequency.

Table 5. Parameters of the 3-ϕ active front-end converter fed 5-ϕ IM drive

Parameters	Values
Phase RMS voltage	230 V
Frequency	50 Hz
Line resistance, inductance	1 ohm, 7 mH
Reactive power (Ref. value)	0
DC bus voltage	400 V
DC link capacitor	760 µF
Switching frequency	3 KHz
Power (P)	1 hp
Input voltage of motor (V)	220
Number of phases, total count poles (p)	5, 4
Stator resistance, inductance	10.1 Ω, 0.833 Henry
Rotor resistance, inductance	9.854 Ω, 0.782 Henry
Mutual inductance	0.782 Henry
Inertia of rotor	0.0088

The 5-ϕ IM fed from the AFEC without a power factor correction control is simulated. Three different sag conditions are simulated and the input current THD, power factor, real power, reactive power, and DC voltage variations are recorded. From Figure 11(a) the 3-ϕ voltage sag condition is observed with a reduction in voltage of 20% between 1 second and 1.3 seconds. The DC link potential is decreasing from 380 V to 282 V, as presented in Figure 11(b).

The power factor is as low as 0.72 because of reasonable reactive power in the system. There is a phase displacement amongst the voltage and current as depicted in Figures 11(c), 11(d), and 11(e), and the variations in torque and speed are undesirable, which can be observed from Figures 11(f) and 11(g). Similar to this, results are obtained for other two cases, and the input current harmonics and power factor are given in Table 6.

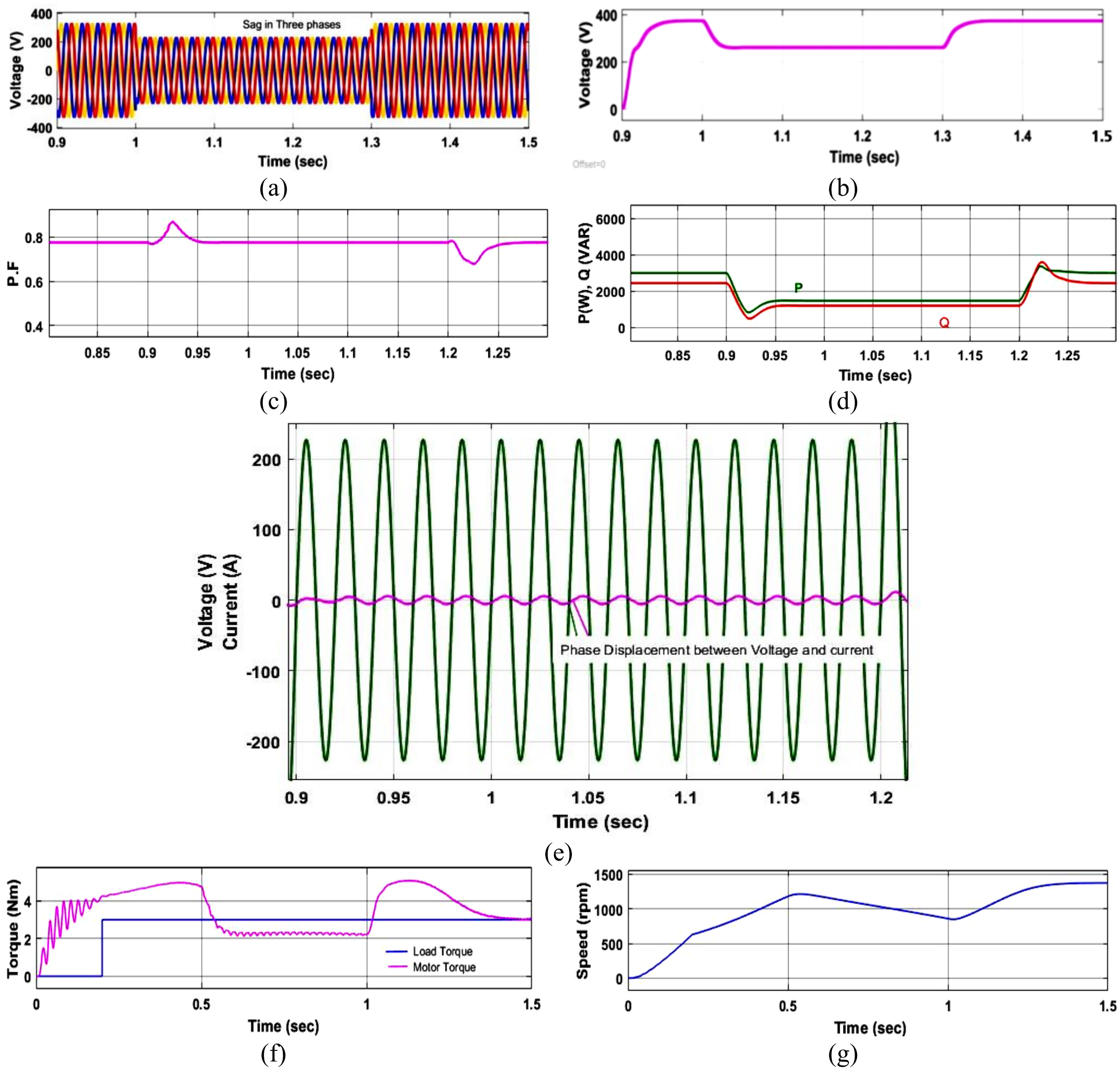

Figure 11. Responses of the 5-ϕ IM drive without AFEC: (a) voltage sag in all phases, (b) DC link voltage, (c) input power factor, (d) real and reactive power, (e) phase relationship between input phase voltage and current, (f) load and motor torque, and (g) speed response

This type of sag greatly affects the input power quality and the output functioning of the system. In order to improve power quality, the AFEC is designed and it is applied for the 5-ϕ IM drive. AFEC with decoupled control in the front end of the 5-ϕ IM drive improves the overall performance of the system. Two types of decouped controls (PI and fuzzy) are proposed and the effectiveness of the control actions are compared.

Figures 12 and 13 indicate the responses of the system under 1-ϕ and 2- ϕ sag conditions. Similar to the previous case, the sag event is noticed between 0.9 and 1.2 seconds. The various responses show that the controllers work better in improving the DC link potential, sinusoidal input current, input power factor, speed, and torque responses of the 5-ϕ IM drive system. The input current, harmonics, and power factor for all cases are presented in Table 6. From the table, the current harmonics for most of the conditions are found to be around 5 % and the corresponding power factor is near unity. These results clearly imply the effictiveness of the FLC's control over the PI controllers. Figure 14 shows the power factor comparison of AFEC with and without controllers.

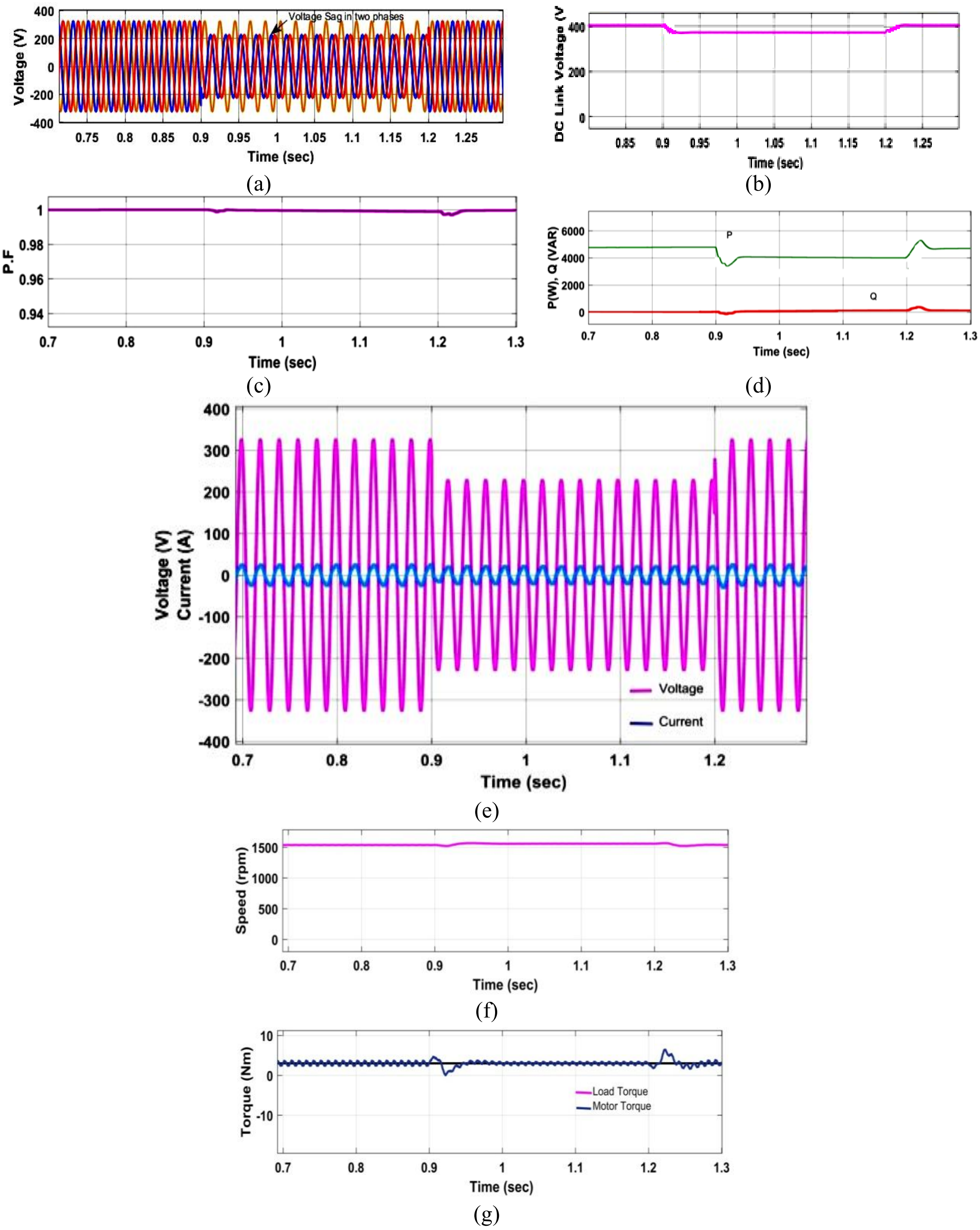

Figure 12. Responses of the 5-ϕ IM fed drive with AFEC: (a) voltage sag in two phases, (b) DC link voltage, (c) input power factor, (d) real and reactive power, (e) phase relationship between input phase voltage and current, (f) load and motor torque, and (g) speed response

Table 6. % THD in input current and power factor

Type of sag		% THD in input current			Power factor
		Phase A	Phase B	Phase C	
Without AFEC	Normal	18.67	18.41	18.57	0.88
	Case A (3-ϕ sag)	20.02	21.12	21.16	0.72
	Case B (2-ϕ sag)	17.27	40.94	45.65	0.786
	Case C (1-ϕ sag)	38.881	18.40	17.7	0.863
AFEC with PI controllers	Normal	7.55	7.59	7.45	0.999
	Case A (3-ϕ sag)	8.07	8.25	7.76	0.87
	Case B (2-ϕ sag)	16.91	27	10.63	0.968
	Case C (1-ϕ sag)	5.02	10.46	12.56	0.991
AFEC with fuzzy controllers	Normal	5.22	5.20	5.26	1
	Case A (3-ϕ sag)	5.4	5.63	5.09	0.997
	Case B (2-ϕ sag)	10.96	11.29	4.7	0.983
	Case C (1-ϕ sag)	4.46	5.89	8.16	0.998

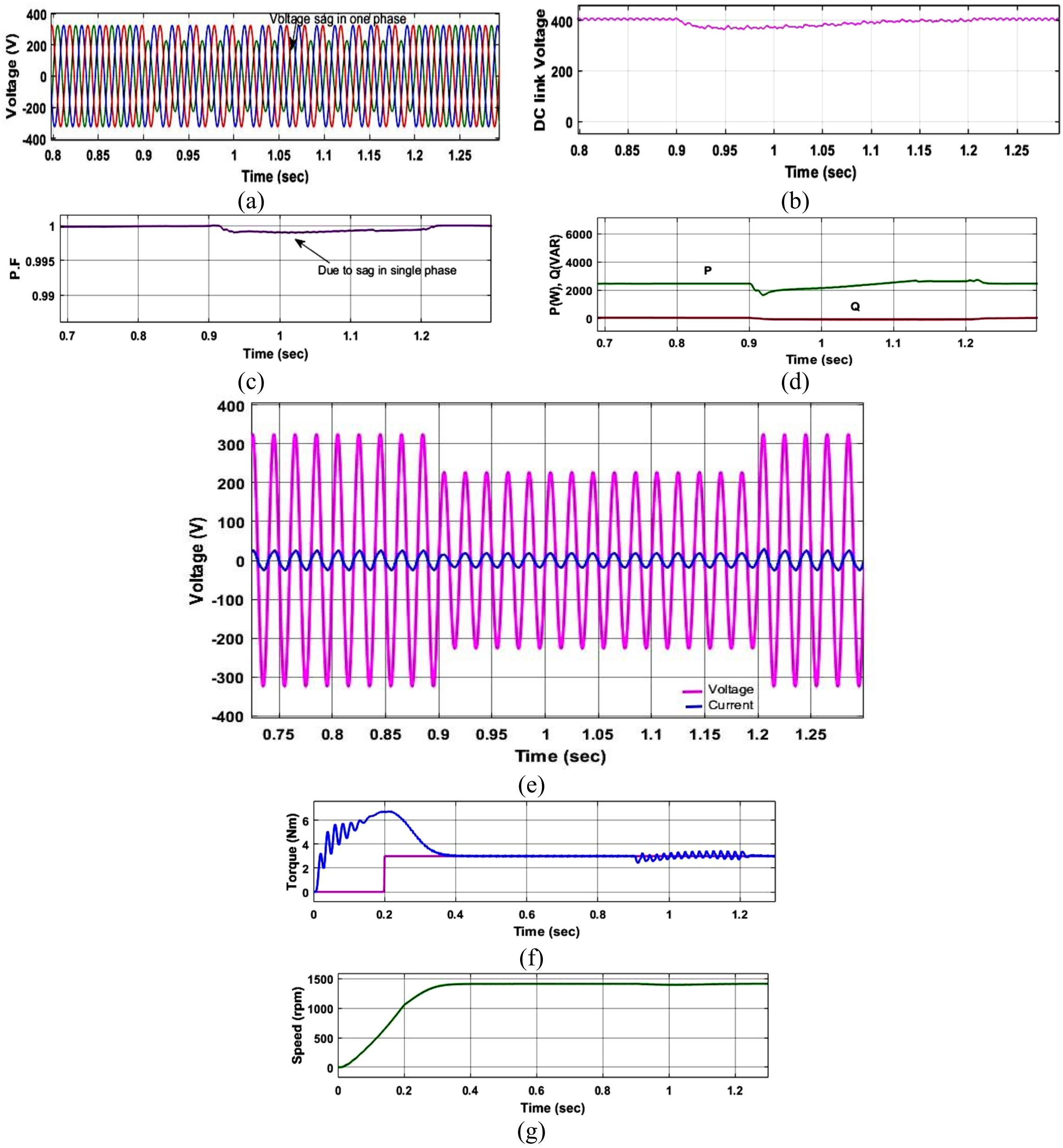

Figure 13. Responses of the 5-ϕ IM drive with AFEC: (a) voltage sag in single phase, (b) DC link voltage, (c) input power factor, (d) real and reactive power, (e) phase relationship between input phase voltage and current, (f) load and motor torque, and (g) speed response

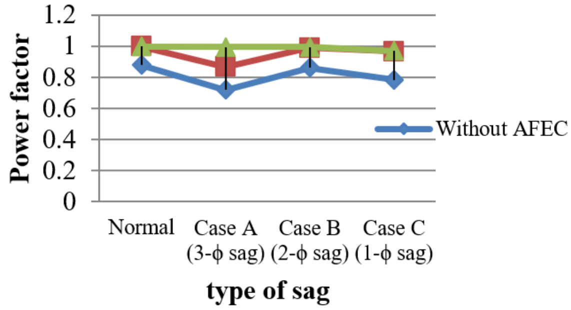

Figure 14. Comparison of power factor for with and without AFEC

8. CONCLUSION

In this paper, an intelligent fuzzy inference system for AFEC has been used to achieve the unity power factor control for a 5-ϕ SVPWM VSI controlled IM fed drive. The behaviour of the multi-phase IM drive changes when supply from the grid is prone to be imbalance situation. The conventional non-linear model is converted into the linear model using non-linear transformation. The designs of decoupled fuzzy controllers are more effective for reactive power minimization, and also, faster dynamic response could be attained in DC as well as reactive power values. This analysis is executed in the MATLAB Simulink for the front-end 5-ϕ SVPWM VSI based IM fed drive. The use of AFEC is able to compensate the voltage disturbance, and simulation results confirm the feasibility of the approach. The comparative evaluation confirms that the fuzzy controller offers enhanced control performance, characterized by reduced input current harmonic distortion and improved power factor under both normal and voltage sag operating conditions. This paper also presents the SVPWM switching scheme for a 5-ϕ VSI fed IM drive to reduce %THD in the output voltage. The SVPWM control for a 5-ϕ VSI provides operation of the drive with minimal THD in output voltages. This control also uses entire DC bus potential and the output responses are better with less magnitude for harmonics of lower order.

FUNDING INFORMATION

No funding involved.

AUTHOR CONTRIBUTIONS STATEMENT

This journal uses the Contributor Roles Taxonomy (CRediT) to recognize individual author contributions, reduce authorship disputes, and facilitate collaboration.

Name of Author	C	M	So	Va	Fo	I	R	D	O	E	Vi	Su	P	Fu
C. Kalaivani	✓	✓	✓	✓	✓	✓		✓	✓	✓			✓	
D. Raja	✓	✓	✓	✓	✓	✓		✓	✓	✓	✓	✓		✓
S. Sivasakthi	✓		✓	✓			✓			✓	✓		✓	✓
R. Gnanaselvam	✓		✓				✓			✓			✓	✓

C : **C**onceptualization
M : **M**ethodology
So : **So**ftware
Va : **Va**lidation
Fo : **Fo**rmal analysis
I : **I**nvestigation
R : **R**esources
D : **D**ata Curation
O : Writing - **O**riginal Draft
E : Writing - Review & **E**diting
Vi : **Vi**sualization
Su : **Su**pervision
P : **P**roject administration
Fu : **Fu**nding acquisition

CONFLICT OF INTEREST STATEMENT

Authors state no conflict of interest.

DATA AVAILABILITY

Data availability is not applicable to this paper as no new data were created or analyzed in this study.

REFERENCES

[1] S. K. Barik and K. K. Jaladi, "Five-phase induction motor DTC-SVM scheme with PI controller and ANN controller," *Procedia Technology*, vol. 25, pp. 816–823, 2016, doi: 10.1016/j.protcy.2016.08.184.

[2] K. B. Yadav, A. K. Mohanty, and P. Kumar, "Recent research trend on multi-phase induction machines," in *Proceedings of the International Conference on Control, Communication and Power Engineering, CCPE*, 2014.

[3] N. Mendoza, J. Pardo, M. Mantilla, and J. Petit, "A comparative analysis of direct power control algorithms for three-phase power inverters," *IEEE Power and Energy Society General Meeting*, 2013, doi: 10.1109/PESMG.2013.6672992.

[4] M. Jamma, M. Barara, M. Akherraz, and B. A. Enache, "Voltage oriented control of three-phase PWM rectifier using space vector modulation and input output feedback linearization theory," in *2016 8th International Conference on Electronics, Computers and Artificial Intelligence (ECAI)*, IEEE, Jun. 2016, pp. 1–8, doi: 10.1109/ECAI.2016.7861085.

[5] C. Heising, M. Oettmeier, R. Bartelt, J. Fang, V. Staudt, and A. Steimel, "Simulation of asymmetric faults of a five-phase induction machine used in naval applications," in *2009 35th Annual Conference of IEEE Industrial Electronics*, IEEE, Nov. 2009, pp. 1298–1303, doi: 10.1109/IECON.2009.5414647.

[6] J. Benzaquen, M. B. Shadmand, A. Stonestreet, and B. Mirafzal, "A unity power factor active rectifier with optimum space-vector predictive dc voltage control for variable frequency supply suitable for more electric aircraft applications," in *2018 IEEE Applied Power Electronics Conference and Exposition (APEC)*, IEEE, Mar. 2018, pp. 1455–1460, doi: 10.1109/APEC.2018.8341208.

[7] P. J. Douglass and I. Trintis, "Balancing distribution systems with three-phase active front end rectifiers: field experiment results," *IET Generation, Transmission & Distribution*, vol. 11, no. 15, pp. 3749–3755, Oct. 2017, doi: 10.1049/iet-gtd.2016.1901.

[8] A. M. Bozorgi, H. Gholami-Khesht, M. Farasat, S. Mehraeen, and M. Monfared, "Model predictive direct power control of three-phase grid-connected converters with fuzzy-based duty cycle modulation," *IEEE Transactions on Industry Applications*, vol. 54, no. 5, pp. 4875–4885, Sept.-Oct. 2018, doi: 10.1109/TIA.2018.2839660.

[9] A. Bouafia, J. -P. Gaubert, and F. Krim, "Predictive direct power control of three-phase pulsewidth modulation (PWM) rectifier using space-vector modulation (SVM)," *IEEE Transactions on Power Electronics*, vol. 25, no. 1, pp. 228–236, Jan. 2010, doi: 10.1109/TPEL.2009.2028731.

[10] Y. Zhang, Z. Li, Y. Zhang, W. Xie, Z. Piao, and C. Hu, "Performance improvement of direct power control of PWM rectifier with simple calculation," *IEEE Transactions on Power Electronics*, vol. 28, no. 7, pp. 3428–3437, 2013, doi: 10.1109/TPEL.2012.2222050.

[11] Y. Zhang, C. Qu, and J. Gao, "Performance improvement of direct power control of PWM rectifier under unbalanced network," *IEEE Transactions on Power Electronics*, vol. 32, no. 3, pp. 2319–2328, Mar. 2017, doi: 10.1109/TPEL.2016.2562262.

[12] J. K. Banda and A. K. Jain, "Single-current-sensor-based active front-end-converter-fed four quadrants induction motor drive," in *Sadhana - Academy Proceedings in Engineering Sciences*, 2017, pp. 1275–1283, doi: 10.1007/s12046-017-0681-1.

[13] T. Gao, S. Zhang, S. Zhang, and J. Zhao, "A dynamic model and modified one-cycle control of three-level front-end rectifier for neutral point voltage balance," *IEEE Access*, vol. 5, pp. 2000–2010, 2017, doi: 10.1109/ACCESS.2017.2668398.

[14] R. Maheshwari, I. Trintis, L. Török, S. Munk-Nielsen, P. J. Douglass, and L. Bede, "A novel high bandwidth current control strategy for sic mosfet based active front-end rectifiers under unbalanced input voltage conditions," *IEEE Transactions on Industrial Electronics*, vol. 64, no. 10, pp. 8310–8320, 2017, doi: 10.1109/TIE.2017.2677325.

[15] W. Taha, A. R. Beig, and I. Boiko, "Quasi optimum pi controller tuning rules for a grid-connected three phase AC to DC PWM rectifier," *International Journal of Electrical Power and Energy Systems*, vol. 96, pp. 74–85, 2018, doi: 10.1016/j.ijepes.2017.09.027.

[16] N. Selvaganesan, D. Raja, and S. Srinivasan, "Fuzzy based fault detection and control for 6/4 switched reluctance motor," *Iranian Journal of Fuzzy Systems*, vol. 4, no. 1, pp. 37–51, 2007.

[17] I. A. Yakimov, S. S. Voronin, E. A. Maklakova, and A. S. Maklakov, "Power quality analysis of hp electric drive based on 3L NPC AFE rectifiers with she modulation method," *Procedia Engineering*, vol. 206, pp. 1843–1847, 2017, doi: 10.1016/j.proeng.2017.10.723.

[18] S. Moinoddin and A. Iqbal, "Space vector model of a five-phase current source inverter," in *2016 - Biennial International Conference on Power and Energy Systems: Towards Sustainable Energy, PESTSE 2016*, 2016, doi: 10.1109/PESTSE.2016.7516470.

[19] D. Sasi, P. J. Kuruvilla, and A. Gopinath, "Generalized SVPWM algorithm for two legged three phase multilevel inverter," *International Journal of Power Electronics and Drive Systems*, vol. 3, no. 3, pp. 279–286, Sep. 2013, doi: 10.11591/ijpeds.v3i3.4099.

[20] D. Zhao, V. S. S. P. K. Hari, G. Narayanan, and R. Ayyanar, "Space-vector-based hybrid pulsewidth modulation techniques for reduced harmonic distortion and switching loss," *IEEE Transactions on Power Electronics*, vol. 25, no. 3, pp. 760–774, Mar. 2010, doi: 10.1109/TPEL.2009.2030200.

[21] S. Galceran, M. Teixidó, A. Sumper, J. Casas, and J. Sánchez, "Adjustable speed drives and power quality," *Renewable Energy and Power Quality Journal*, vol. 1, no. 1, pp. 256–261, 2003, doi: 10.24084/repqj01.364.

[22] W. N. Wan Abdul Munim, M. F. Ismail, A. F. Abidin, and H. Che Mat Haris, "Multi-phase inverter space vector modulation," in *Proceedings of the 2013 IEEE 7th International Power Engineering and Optimization Conference, PEOCO 2013*, 2013, pp. 149–154, doi: 10.1109/PEOCO.2013.6564533.

[23] J. K. Nayak, S. B. Sahoo, R. K. Behera, and B. Chikondra, "Analytical study on fault-tolerant control of five-phase induction motor drive," in *2025 IEEE Energy Conversion Congress and Exposition Asia: Shaping a Greener Future with Power Electronics, ECCE-Asia 2025*, 2025, doi: 10.1109/ECCE-Asia63110.2025.11111774.

[24] E. Levi, N. Bodo, O. Dordevic, and M. Jones, "Recent advances in power electronic converter control for multiphase drive systems," in *Proceedings - 2013 IEEE Workshop on Electrical Machines Design, Control and Diagnosis, WEMDCD 2013*, 2013, pp. 158–167, doi: 10.1109/WEMDCD.2013.6525176.

[25] U. Mahanta, B. C. Mohanta, A. K. Panda, and B. P. Panigrahi, "Fuzzy logic-based direct torque control for improvement of the fault-tolerant drive of a five-phase induction motor," *Transactions of the Institute of Measurement and Control*, vol. 43, no. 14, pp. 3120–3128, 2021, doi: 10.1177/01423312211015556.

BIOGRAPHIES OF AUTHORS

Dr. C. Kalaivani received her B.Tech. degree in electrical and electronics engineering and M.Tech. degree in electrical drives and control from Pondicherry Engineering College, Pondicherry University, Pondicherry, India, in 2004 and 2008, respectively. She received her Ph.D. degree in electrical engineering from Pondicherry University in 2020. She worked as quality engineer at India Nippon Electricals Limited from 2004 to 2006. She worked as an assistant professor in Sri Manakula Vinayagar Engineering College from 2008 to 2014. Currently, she is working as an associate professor at AMET University, Chennai. She has published more than 30 research papers in various conferences and journals. Her research interests include wind energy conversion systems, electric vehicles, power electronic circuits and electric drives, power electronic applications in power systems, and renewable energy systems. She can be contacted at email: dr.kalaivani@amet-ist.in.

Dr. D. Raja received his B.Tech. degree in electrical and electronics engineering in 2004; his M.Tech. degree in electrical drives and control in 2006 and Ph.D. in 2020 from Pondicherry Engineering College, Pondicherry University. He is working as a professor in the Department of Electrical and Electronics Engineering, Sri Manakula Vinayagar Engineering College, Pondicherry, and he has 19 years of teaching experience in the same institute. His research area includes power electronics converters, electrical drives and control, and power electronic applications in power systems. He can be contacted at email: rajaapeee@smvec.ac.in.

Dr. S. Sivasakthi received the B.E. degree in electrical and electronics engineering from the University of Madras, Madras, 1999; the M.E. degree in power system from the Annamalai University, Chidambaram, India, 2008; and the Ph.D. degree in electrical and electronics engineering from the Annamalai University, Chidambaram, India, in 2019. He is a professor and head of Electrical and Electronics Engineering at the Krishnasamy College of Engineering and Technology, Cuddalore, India. He has authored more than 35 research articles in various international journals and conferences. His research interests include economic dispatch, unit commitment, regulated and deregulated power systems, state estimation, and renewable energy systems. He has more than 24 years of teaching experience. He can be contacted at email: sivasakthi_gayu@yahoo.co.in.

Dr. R. Gnanaselvam received a Bachelor of Engineering in electronics and communication engineering (ECE) from R.M.K. Engineering College, University of Madras, Chennai, and a Master of Technology in embedded system technology from SRM University, Chennai, Tamil Nadu, India, in 2003 and 2014, respectively. He completed a Ph.D. in evaluation and optimization of coverage enhancement methods for NB-IoT and LoRa in the Department of Electronics and Communication Engineering, SRM Institute of Science and Technology, Kattankulathur, Chennai, in 2026. His research interests include the low power wide area networks, 5G communications, image processing, internet of things (IoT), machine learning, and embedded system technology, and he has published more than 13 papers in reputed international journals and conferences. He can be contacted at email: gnanaselvam@kveg.in.